J. Fluid Mech. (2010), *vol.* 656, *pp.* 29–50.
doi:10.1017/S0022112010001011

A study of the flow structure for Mach reflection in steady supersonic flow

B. GAO AND Z. N. WU†

Department of Engineering Mechanics, Tsinghua University, Beijing 100084, P.R. China

(Received 25 October 2009; revised 22 February 2010; accepted 23 February 2010; first published online 21 May 2010)

In this paper we study the waves generated over the slipline and their interactions with other waves for Mach reflection in steady two-dimensional supersonic flow. We find that a series of expansion and compression waves exist over the slip line, even in the region immediately behind the leading part of the reflected shock wave, previously regarded as a uniform flow. These waves make the leading part of the slipline, previously regarded as straight, deviate nonlinearly towards the reflecting surface. When the transmitted expansion waves from the upper corner first intersect the slipline, an inflexion point is produced. Downstream of this inflexion point, compression waves are produced over the slipline. By considering the interaction between the various expansion or compression waves, we obtain a Mach stem height, the shape and position of the slipline and reflected shock wave, compared well to computational fluid dynamics (CFD) results. We also briefly consider the case with a subsonic portion behind the reflected shock wave. The global flow pattern is obtained through CFD and the starting point of the sonic line is identified through a simple analysis. The sonic line appears to coincide with the first Mach wave from the upper corner expansion fan after transmitted from the reflected shock wave.

1. Introduction

It is well known that the reflection of oblique shock waves over a horizontal plane results in two types of wave configurations, regular reflection (RR) and Mach reflection (MR). The phenomenon of MR was first observed by Mach (1878). A considerable number of studies have been made for when and how both types of reflection occur. Von Neumann (1943, 1945) developed the three-shock theory and proposed two transition criteria from RR to MR and vice versa: the reflected shock wave detachment criterion and the mechanical equilibrium criterion, or von Neumann criterion. These two criteria are separated by a zone now called dual solution domain, where both RR and MR are possible (Henderson & Lozzi 1975, 1979; Hornung & Robinson 1982; Chpoun *et al.* 1994, 1995; Vuillon, Zeitoun & Ben-Dor 1995; Teshukov 1989; Li & Ben-Dor 1996). Whether it is an RR or an MR in the dual solution domain depends on the history that the actual steady flow is built (Hornung, Oertel & Sandeman 1979; Chpoun *et al.* 1995; Ivanov, Gimelshein & Beylich 1995; Shirozu & Nishida 1995; Ben-Dor, Elperin & Vasiliev 2003).

Figure 1 identifies various regions pertaining to the free-stream Mach number M_0 and wedge angle θ_w. MR can only occur for $\theta_w^N \leqslant \theta_w \leqslant \theta_w^M$, where θ_w^N is von Neumann criterion and θ_w^M is the incident shock wave detachment criterion. In case of MR,

† Email address for correspondence: ziniuwu@tsinghua.edu.cn

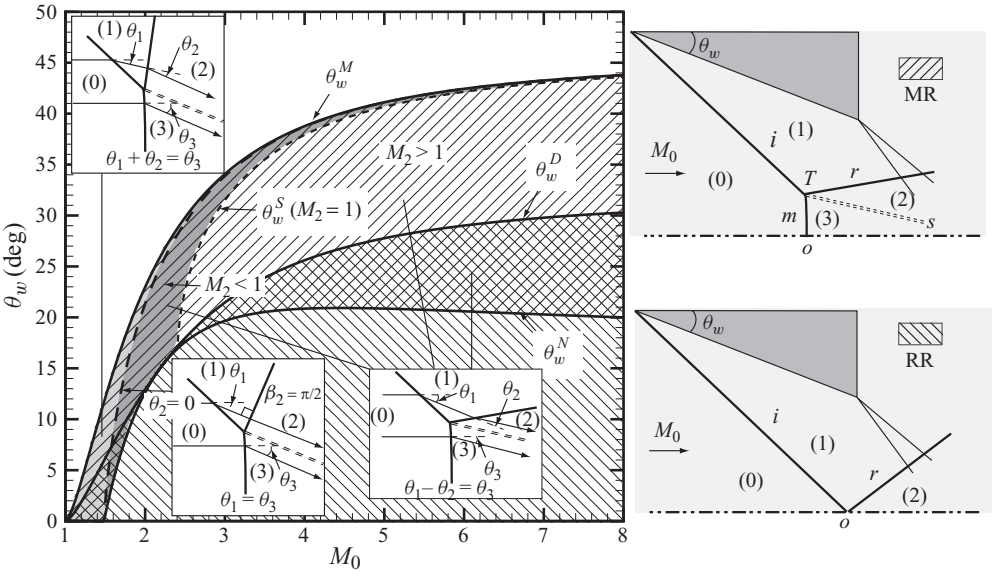

FIGURE 1. Domains of different types of reflection in the (M_0, θ_w)-plane, and RR and MR.

a triple point (T) exists which connects the incident shock wave (i), reflected shock wave (r), Mach stem (m) and slipline (s). The flow behind the reflected shock is supersonic ($M_2 > 1$) for $\theta_w < \theta_w^S$ and subsonic ($M_2 < 1$) for $\theta_w < \theta_w^S$ (Chow & Chang 1974), where θ_w^S corresponds to the wedge angle at which $M_2 = 1$. A three-shock configuration is called 'standard' if $\theta_1 - \theta_2 = \theta_3$, and 'non-standard' if $\theta_1 + \theta_2 = \theta_3$ (Ben-Dor 2007). These two cases are separated by the line $\theta_2 = 0$ (figure 1).

A number of studies have been devoted to the position of the triple point (T), Mach stem height (H_m) and shape of the waves. Chow & Chang (1974) studied the Mach stem for nozzle free jet problem, where the expansion fan comes from the reflection of the reflected shock wave over a free surface. Azevedo (1989) and Azevedo & Liu (1993) developed a model for predicting H_m (see figure 2*a*). They assumed that the sonic throat occurs where the leading Mach wave of the expansion fan intersects the slip stream. They considered the subsonic pocket to be an isotropically quasi-one-dimensional converging ideal gas flow and the slipline from the triple point to the sonic throat to be a straight line. They applied von Neumann's three-shock theory for the triple point T and the quasi-one-dimensional isentropic relation for the subsonic pocket $TOKE$.

Li & Ben-Dor (1997) allowed the sonic throat to occur further downstream (see figure 2*b*) and assumed that the Mach stem (m), the reflected shock wave (r) and the slipline (s) are slightly curved. They ignored the influence of the reflected waves when the transmitted expansion waves (BF or CE) strike the slipline.

Recently, Mouton & Hornung (2007) studied the growth rate of the Mach stem height during the RR $\rightarrow$ MR transition. When the transition is finished, the Mach stem height is the steady-state one. They assumed that the Mach stem (TO), the reflected shock wave (TB), the slipline (TE) and the Mach waves (RC, CE) all maintain a straight line (see figure 2*c*) during the transition. They obtained the height of the Mach stem using the geometrical relationship established between straight segments AT, TC, RC, CE, EK and model-scale quantities w, H_0.

The above models provide useful and fast way to determine the Mach stem height.

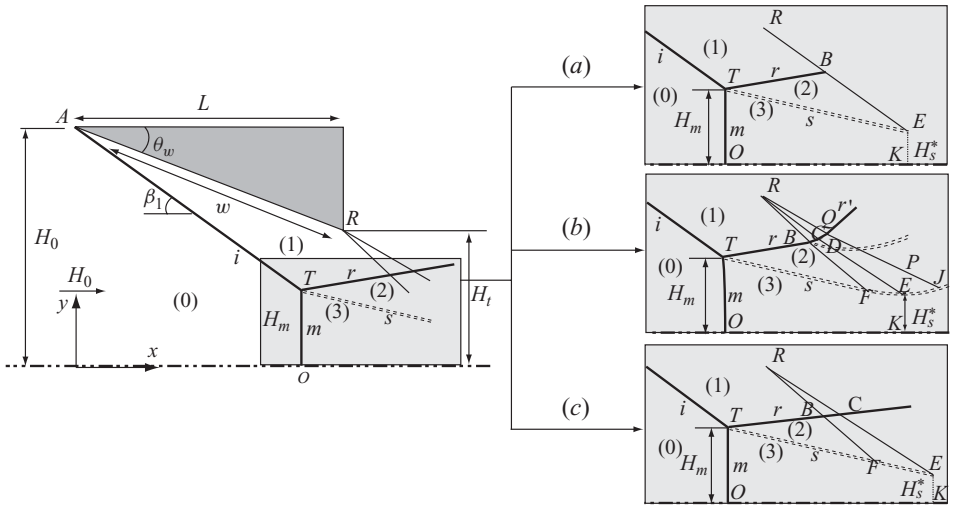

FIGURE 2. Schematic illustration of the MR configuration used by (*a*) Azevedo & Liu (1993), (*b*) Li & Ben-Dor (1997) and (*c*) Mouton & Hornung (2007).

The shape of the Mach stem has been early studied experimentally for pseudo-steady reflections (Dewey & McMillin 1985*a*, *b*; Olim & Dewey 1992; Dewey & Barss 1996). The shape of the Mach stem has also been studied by Li, Ben-Dor & Han (1994) for pseudo-steady reflections, and by Li & Ben-Dor (1997) for steady flows using a geometrical point of view. Tan, Ren & Wu (2006) performed an analysis of the subsonic flow pocket immediately behind the Mach stem and derived the relation $(x+\sqrt{R^2-H_m^2})^2+y^2=R^2$ for the shape of the Mach stem. Here $R=(\alpha/\theta_3)H_m$ with $\alpha=2\left(M_0^2-1\right)/(2+(\gamma-1)M_0^2)$. Hence, the Mach stem is a circular arc centred at $(-\sqrt{R^2-H_m^2},0)$.

Despite the previous contributions, there still remain some unresolved issues which we believe important. First, the previous models yield H_m, though with a good precision in comparison with the simplicity of the model, either too small or too large in comparison with the CFD results. It seems that some important physics were not considered. Second, CFD results (§ 2.1) show that the flow immediately behind the leading part of the reflected shock wave is not a uniform one, in contrast to what we have normally assumed. Is this simply numerical error in CFD or is there a physical reason behind it? Third, there was no study about the shape and positions of the slipline and reflected shock waves, though Dewey & McMillin (1985*a*, *b*) measured the shapes of the incident, reflected and Mach stem shocks for the pseudo-steady cases.

In § 2, we will show through CFD that the flow immediately behind the leading part of the reflected shock wave is not uniform in contrast to what we have assumed in the previous studies. We then relate this non-uniformity to expansion waves produced over the leading part of the slipline for the case $M_2>1$ and to the pressure decrease below the slipline for the case $M_2<1$. The production of other waves and their interactions with other waves are also described.

For the case $M_2>1$, a global algorithm is built to solve the entire problem, including the shape of the slipline and reflected shock wave, the overall solution and the Mach stem height. The results are presented and analysed in § 3, where we also briefly consider the case $M_2<1$, for which there is the difficult problem of the shape of the sonic line.

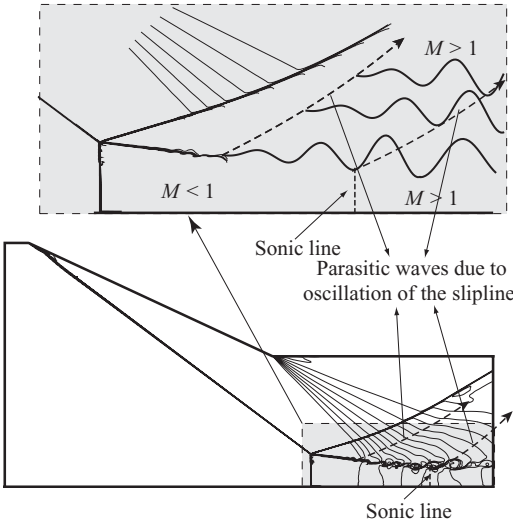

FIGURE 3. Wavy nature of the slipline due to Kelvin–helmholtz instability and parasitic waves.

2. Flow structure of Mach reflection

2.1. *Details of the Mach reflection configuration*

We begin with displaying refined CFD results, using the same numerical method as in Tan *et al.* (2006), proposed by Ren (2003), to show that waves, previously not observed, are produced over the slipline. We then describe the various flow structures that exist in MR.

Even though current CFD method can well be used to compute MR, there is the grid refinement inconvenience. The grid should be refined enough to have more accurate solution. But if the grid is fine enough, the slipline will display Kelvin–helmholtz instability (Samtaney & Pullin 1996; Ivanov *et al.* 2002) due to numerical viscosity. The rolling of the slipline will produce parasitic waves (figure 3) which spoil CFD results. In the subsequent (theoretical) study, we will disregard the rolling up of the slipline.

In figure 4(a) we display the density contour lines for two kinds of mesh density (300×200 and 600×400) under the flow conditions $M_0 = 2.84, \theta_w = 20.8$ and $w/H_0 = 1.42$. The overall configurations are very similar to each other except for the regions near the slipline, where the transmitted Mach waves with the refined grid are deformed due to the curl of the slipline. The normalized Mach stem height is 0.191 using both of the two kinds of mesh density. Figure 4(b) shows the comparison for $M_0 = 4.5, \theta_w = 25$ and $w/H_0 = 1.1$, where the normalized Mach stem height is 0.131 and 0.132 using coarse grid and refined grid, respectively. Since there is no essential difference of results between the two grids, the mesh density 300×200 is used throughout the rest of this paper.

Now we display in figure 5 the density, pressure and Mach number contours for two flow conditions. We observe non-uniformity of the flow immediately behind the leading part of the reflected shock wave, which is nevertheless regarded as uniform in all the previously studies. Figure 5(a) corresponds to the case where the flow behind the reflected shock wave is purely supersonic. We observe a series of expansion waves over the leading part of the slipline. Figure 5(b) corresponds to the case for which

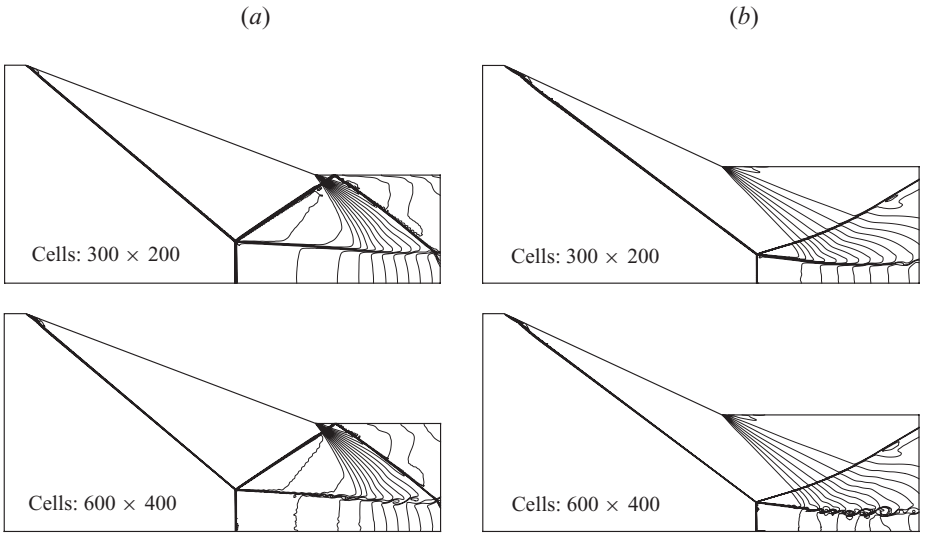

FIGURE 4. Density contours showing the structure of the MR in the gird refinement study. (*a*) $M_0 = 2.84, \theta_w = 20.8^{\circ}, w/H_0 = 1.42$, (*b*) $M_0 = 4.5, \theta_w = 25, w/H_0 = 1.1$.

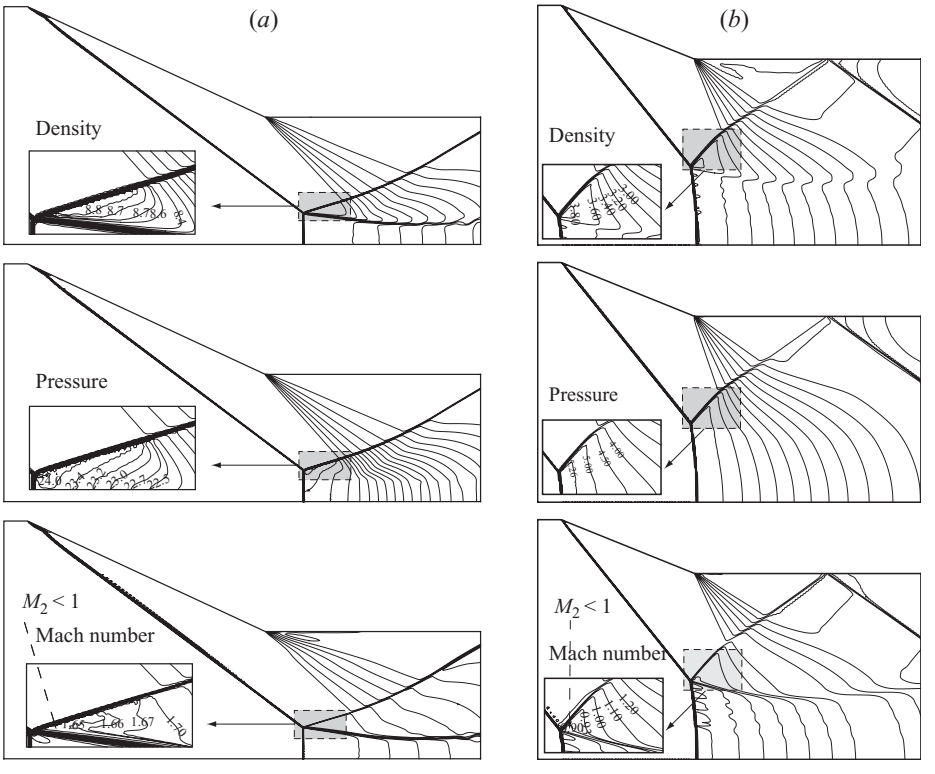

FIGURE 5. Contours for MR ($\Delta x/H_0 = 0.003$). (*a*) The flow behind the reflected shock wave is purely supersonic, $M_0 = 4.5, \theta_w = 25^{\circ}, w/H_0 = 1.1$ and (*b*) there is a subsonic flow behind the reflected shock wave, $M_0 = 2.2, \theta_w = 22^{\circ}, w/H_0 = 0.6$.

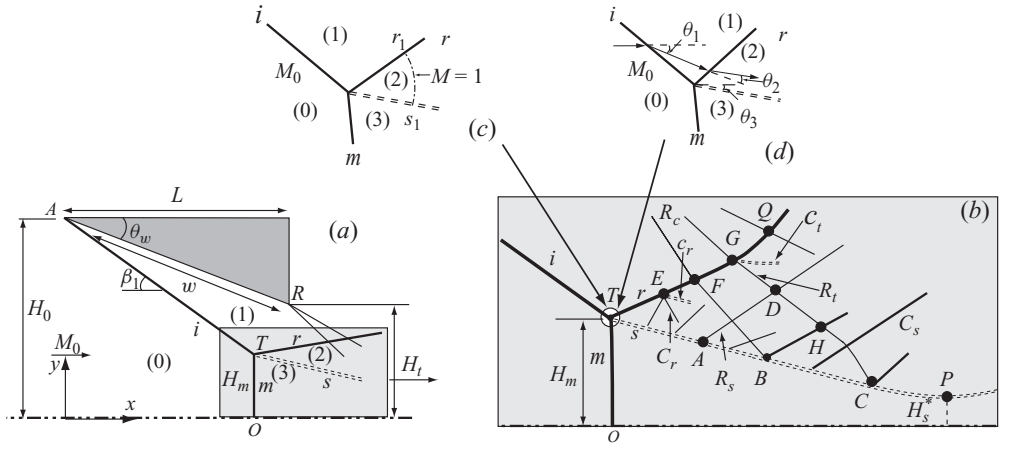

FIGURE 6. Schematic illustration of the Mach reflection wave configuration.

there is a subsonic flow behind the reflected shock wave, the flow then transits from subsonic to supersonic.

The non-uniformity behind the reflected shock wave in fact has a physical background. The left part of the slipline, normally regarded as a straight line, is in fact subjected to the influence of varying pressure in the flow tube between the reflecting surface and the slipline. Since the slipline firstly deviates towards the reflecting surface, this tube is convergent along the flow direction. Hence the pressure continuously decreases, according to the quasi-one-dimensional-flow theory for subsonic flow. In order to balance this pressure decrease, expansion waves must be produced above the slipline, which makes the flow become non-uniform in the region immediately behind the reflected shock wave, and makes the slipline further deviate towards the reflecting surface on the other hand. This means the slipline is not a straight one.

In figure 6 we sketch the MR configuration including waves produced over the slipline and their interaction with other flow structure.The basic flow structures include the reflected shock wave (r), the slipline (s), the Mach stem (m), the triple point (T), expansion waves (R_c) by the upper corner. The interaction of R_c with r, for instance, at point G, produces transmitted Mach waves (R_t) and slipline (c_t).

The pressure decrease along the slipline, for instance, at point A, produces a series of expansion waves (R_s). The reflection of R_t over the slipline, for instance, at point C, produces reflected waves (C_s). Apparently, it is not clear whether C_s is a compression or an expansion wave. In § 3, we will show that C_s is always compressive even near the point B. The reflection of R_s over the reflected shock (r), for instance, at point E, produces reflected expansion or compression waves (C_r) and sliplines (c_r). The expansion waves R_s and the compression waves C_s also intersect the transmitted waves (R_t), for instance, at point D and H, respectively. When $M_2 < 1$, a sonic line ($M = 1$) also exists (figure 6c). The position of the sonic line (s_1 and r_1) and its shape are new features compared to the case $M_2 > 1$.

2.2. *Physical model for the case* $M_2 > 1$

Here, we describe the physical model to describe the various flow structure as sketched in figure 6. This model will be used to build an algorithm for the shape of slipline, reflected shock wave and Mach stem height. Following conventional notations, we

use ρ, p, V, a, M, γ to denote the density, pressure, velocity, sound speed, Mach number and ratio of specific heats of the gas, respectively. We also use β and θ to denote the shock angle and flow deflection angle across an oblique shock wave. In this section we only consider the case $M_2 > 1$, and the situation with $M_2 < 1$ will be briefly considered in § 3.3.

2.2.1. *Recall of shock relations and three-shock theory*

For oblique shock waves connecting the downstream flow (with subscript '1') to the upstream one (with subscript '0'), the following classical shock relations hold

$$\left.\begin{aligned} M_1^2 = f(M_0, \beta_1),\ p_1/p_0 = g(M_0, \beta_1),\ \rho_1/\rho_0 = h(M_0, \beta_1), \\ a_1/a_0 = A(M_0, \beta_1),\ S(M_0, \beta_1, \theta_1) = 0, \end{aligned}\right\} \tag{2.1}$$

where

$$f(M, \beta) \equiv \frac{M^2 + \dfrac{2}{\gamma - 1}}{\dfrac{2\gamma}{\gamma - 1} M^2 \sin^2\beta - 1} + \frac{M^2 \cos^2\beta}{\dfrac{\gamma - 1}{2} M^2 \sin^2\beta + 1},$$

$$g(M, \beta) \equiv \frac{2\gamma}{\gamma + 1} M^2 \sin^2\beta - \frac{\gamma - 1}{\gamma + 1},$$

$$h(M, \beta) \equiv \frac{(\gamma + 1) M^2 \sin^2\beta}{(\gamma - 1) M^2 \sin^2\beta + 2},$$

$$A(M, \beta) \equiv \frac{\left[(\gamma - 1) M^2 \sin^2\beta + 2\right]^{1/2} \left[2\gamma M^2 \sin^2\beta - (\gamma - 1)\right]^{1/2}}{(\gamma + 1) M \sin\beta}$$

and

$$S(M, \beta, \theta) \equiv 2\cot\beta \frac{M^2 \sin^2\beta - 1}{M^2(\gamma + \cos 2\beta) + 2} - \tan\theta.$$

In the well-known triple-point theory, the shock relation (2.1) is applied, at the triple point (T), across the incident shock (i) for weak solution, the reflected shock wave (r) for weak solution normally, but at the case $M_2 < 1$, for strong solution, and the Mach stem (m) for strong solution. The pressure across the slipline is continuous $p_2 = p_3$, and the flow deviation angles satisfy $\theta_3 = \theta_1 - \theta_2$ for 'standard' three-shock configuration and $\theta_3 = \theta_1 + \theta_2$ for 'non-standard' three-shock configuration. The equations can be solved by an iterative process starting from an initial guess for the angle θ_2.

2.2.2. *Expansion and compression waves produced over the slipline*

In figure 7 we display the production of expansion or compression waves over the slipline. The pressure decrease along the flow tube below the slipline, when approximated by the quasi-one-dimensional flow theory, is related to the sectional height or the y position of the slipline (H_s) of the tube by

$$\frac{\mathrm{d}p}{p} = \frac{\gamma M_b^2}{1 - M_b} \frac{\mathrm{d}H_s}{H_s}. \tag{2.2}$$

Here M_b is the Mach number below the slipline (averaged over the height in the quasi-one-dimensional flow theory).

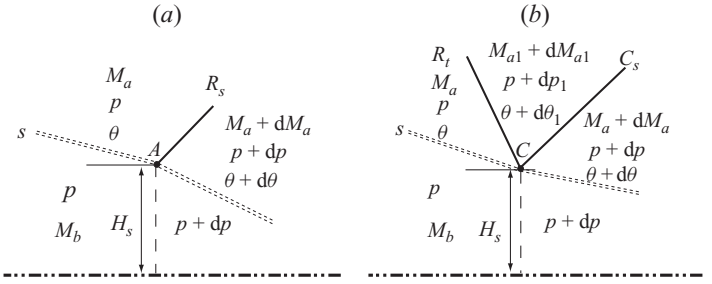

FIGURE 7. Expansion and compression waves produced over the slipline. (a) Expansion waves (R_s), and (b) compression waves (C_s).

The sectional height H_s, at any position with a Mach number M_b, is related to the height H_s^* of the sonic throat through

$$\frac{H_s}{H_s^*} = \sigma(M_b), \quad \sigma(M) = \frac{1}{M}\left(1 + \frac{\gamma - 1}{2}M^2\right)^{(\gamma+1)/(2(\gamma-1))}. \tag{2.3}$$

Geometrically, the variation of H_s can be expressed also as a function of the local angle of the slipline

$$\mathrm{d}H_s = -\theta \mathrm{d}x. \tag{2.4}$$

Considering figure 7(a), the variation of the angle θ produces expansion (Mach) waves (R_s) over the slipline. Let the local Mach number immediately above the slipline be M_a, we have the following classical relations for expansion waves

$$\mathrm{d}\theta = \nu(M_a + \mathrm{d}M_a) - \nu(M_a), \frac{p + \mathrm{d}p}{p} = \chi(M_a, M_a + \mathrm{d}M_a), \sin\mu_a = \frac{1}{M_a}, \tag{2.5}$$

where μ is the Mach angle, and $\nu(M)$ is the Prandtl–Meyer function

$$\nu(M) = \sqrt{\left(\frac{\gamma+1}{\gamma-1}\right)}\arctan\sqrt{\left[\frac{\gamma-1}{\gamma+1}(M^2-1)\right]} - \arctan\sqrt{(M^2-1)}$$

and

$$\chi(M_0, M_1) = \left(\frac{2 + (\gamma-1)M_0^2}{2 + (\gamma-1)M_1^2}\right)^{\gamma/(\gamma-1)}.$$

Once H_s^* is given, the above equations, which form a closed set, can be used to determine the shape of the slipline before it intersects the transmitted waves (R_t), as well as the intensity and direction of the expansion waves (R_s).

Now consider the slipline after the transmitted waves intersect it (after point B). Below the slipline, the relations (2.2)–(2.4) still hold. The pressure variation $\mathrm{d}p$ below the slipline is balanced by both the incident transmitted wave (R_t) and the reflected compression wave (C_s). The flow parameters between R_t and C_s satisfy

$$\mathrm{d}\theta_1 = \nu(M_a + \mathrm{d}M_{a1}) - \nu(M_a), \quad \frac{p + \mathrm{d}p_1}{p_a} = \chi(M_a, M_a + \mathrm{d}M_{a1}), \quad \sin\mu_a = \frac{1}{M_a}. \tag{2.6}$$

Actually, the intensity and direction of the incident wave (R_t) and $M_a + \mathrm{d}M_{a1}$, $p + \mathrm{d}p_1$, $\theta + \mathrm{d}\theta_1$ are determined by the interaction of the waves R_t with C_s, which will be described in § 2.2.4. Thus, we do not have to use (2.6) to obtain $M_a + \mathrm{d}M_{a1}$, $p + \mathrm{d}p_1$, $\theta + \mathrm{d}\theta_1$.

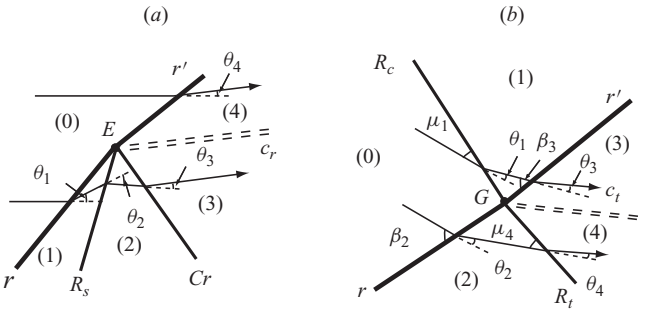

FIGURE 8. Transmitted and reflected waves from the reflected shock wave. (*a*) *Rs* reflects from *r*, and (*b*) *Rc* transmits from the *r*.

Assume C_s to be a compression wave, we may use the following shock relation for C_s

$$\left.\begin{aligned}(M_a + \mathrm{d}M_a)^2 &= f\left(M_a + \mathrm{d}M_{a1}, \beta_{C_s}\right),\\ \frac{p + \mathrm{d}p}{p + \mathrm{d}p_1} &= g\left(M_a + \mathrm{d}M_{a1}, \beta_{C_s}\right),\\ S\left(M_a + \mathrm{d}M_{a1}, \beta_{C_s}, \mathrm{d}\theta - \mathrm{d}\theta_1\right) &= 0.\end{aligned}\right\} \tag{2.7}$$

One may also use the Prandtl–Meyer relation (2.5) for C_s. In case that θ varies smoothly, both types of relations yield the same results. The above three relations, for the four parameters $\mathrm{d}M_a$, $\mathrm{d}p$, $\mathrm{d}\theta$ and β_{C_s} should be supplemented by one more relation evolved from (2.2)–(2.4), that is,

$$\frac{\mathrm{d}p}{p} = -\frac{\gamma M_b^2}{1 - M_b}\frac{\theta}{H_s}\mathrm{d}x, \tag{2.8}$$

where H_s satisfies (2.3).

2.2.3. *Transmitted and reflected waves from the reflected shock wave*

Considering figure 8(*a*), the expansion wave R_s, when striking the reflected shock wave r, produces a reflected expansion or compression wave (C_r) and a slipline (c_r). Before interacting with R_s, the flow parameters immediately behind r satisfy

$$M_1^2 = f(M_0, \beta_1), \quad p_1/p_0 = g(M_0, \beta_1), \quad S(M_0, \beta_1, \theta_1) = 0. \tag{2.9}$$

Knowing the intensity and direction of the incident wave r, we can obtain the flow parameters in region 1. Across R_s we have the Plandtl–Meyer relations

$$\nu(M_2) - \nu(M_1) = \theta_2, \quad p_2/p_1 = \chi(M_1, M_2). \tag{2.10}$$

Then the flow parameters after C_r satisfy

$$\nu(M_3) - \nu(M_2) = \theta_3, \quad p_3/p_2 = \chi(M_2, M_3). \tag{2.11}$$

Apparently, it is not clear whether C_s is an expansion wave or a compression wave. When solving the above equation, $\theta_3 > 0$ corresponds to an expansion wave and $\theta_3 < 0$ corresponds to a compression wave.

After interacting with R_s, the intensity of the reflected shock (r') become a little weaker, across which the shock relation gives

$$M_4^2 = f(M_0, \beta_4), \quad p_4/p_0 = g(M_0, \beta_4), \quad S(M_0, \beta_4, \theta_4) = 0. \tag{2.12}$$

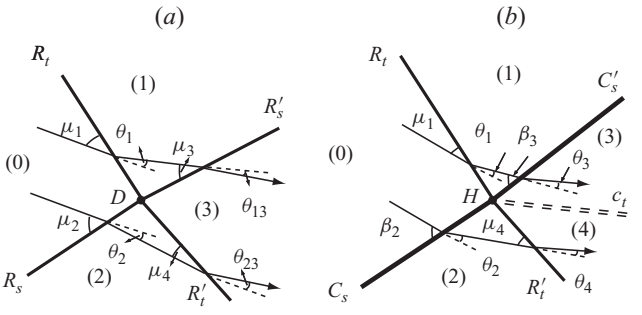

FIGURE 9. Interaction between the transmitted waves R_t and the waves, (a) R_s and (b) C_s, from the slipline.

The above five relations equation (2.11)–(2.12), for the seven parameters M_3, p_3, θ_3, M_4, p_4, θ_4 and β_4, should be supplemented by the pressure and deflection angle continuity across the slipline (c_r),

$$\theta_1 - \theta_2 + \theta_3 = \theta_4, \quad p_3 = p_4. \tag{2.13}$$

The expansion wave R_c transmitting from the reflected shock wave r (figure 8b) produces a transmitted expansion wave (R_t), a slipline (c_t) and a transmitted shock wave (r'). Before interacting with each other, the flow parameters immediately behind R_c satisfy

$$\nu(M_1) - \nu(M_0) = \theta_1, \;\; p_1/p_0 = \chi(M_0, M_1), \tag{2.14}$$

and the flow parameters immediately behind r satisfy

$$M_2^2 = f(M_0, \beta_2), \;\; p_2/p_0 = g(M_0, \beta_2), \;\; S(M_0, \beta_2, \theta_2) = 0. \tag{2.15}$$

The intensity and direction of the incident wave R_c and r are given, so that from (2.14) and (2.15) the flow parameters in region 1 and 2 can be obtained.

Across the transmitted expansion wave and shock, the parameters satisfy

$$\nu(M_4) - \nu(M_2) = \theta_4, \;\; p_4/p_2 = \chi(M_2, M_4), \tag{2.16}$$

$$M_3^2 = f(M_1, \beta_3), \;\; p_3/p_1 = g(M_1, \beta_3), \;\; S(M_1, \beta_3, \theta_3) = 0. \tag{2.17}$$

The above five relations, for the seven parameters M_3, p_3, β_3, θ_3, M_4, p_4 and θ_4, should be supplemented by the pressure and deflection angle continuity,

$$\theta_1 + \theta_3 = \theta_2 + \theta_4, \quad p_3 = p_4. \tag{2.18}$$

2.2.4. *Interaction between the transmitted waves and the waves generated from the slipline*

The flow region formed by the slipline (s), reflected shock wave (r) and the first transmitted wave (FB in figure 6) is a region full of wave interactions. Considering figure 9(a), the interaction between the transmitted expansion wave R_t and the expansion wave R_s produces two more transmitted expansion wave R'_t and R'_s. Knowing the intensity and direction of the incident waves, the flow parameters immediately behind them (region 1 and 2) satisfy

$$\left.\begin{aligned} \nu(M_1) - \nu(M_0) = \theta_1, \;\; p_1/p_0 = \chi(M_0, M_1), \\ \nu(M_2) - \nu(M_0) = \theta_2, \;\; p_2/p_0 = \chi(M_0, M_2). \end{aligned}\right\} \tag{2.19}$$

Across the transmitted expansion waves, the parameters satisfy

$$\left.\begin{aligned} \nu(M_3) - \nu(M_1) &= \theta_{13}, \quad p_3/p_1 = \chi(M_1, M_3), \\ \nu(M_3) - \nu(M_2) &= \theta_{23}, \quad p_3/p_2 = \chi(M_2, M_3). \end{aligned}\right\} \tag{2.20}$$

Across the expansion wave, the flow is isentropic. Thus, only three equations of the above four are independent. We need supplement a relation for deflection angle continuity,

$$\theta_1 - \theta_{13} = -\theta_2 + \theta_{24}. \tag{2.21}$$

Now we consider the interaction of R_t and C_s (figure 9*b*). Comparing with a shock wave, the intensity of the compression C_s is more weaker, but the shock wave relation (2.1) still holds. Thus, the interaction of R_t and C_s is the same as the interaction of R_t and r (§ 2.2.3).

2.2.5. *Overall algorithm*

Now we describe the global algorithm used to obtain the slipline and reflected shock wave. Only the important waves and their interactions are retained. The reflected waves C_s due to the impingement of R_s on the reflected shock wave and the sliplines c_t due to interaction between R_t and C_s are supposed to have very weak influence so that they are simply ignored.

The overall solution process are described now. First, assume that we have an initial guess of the Mach stem height H_m^*, from which we also have an initial value for the position of the triple point (x_T, y_T). From the quasi-one-dimensional-flow theory, the height H_s^* of the sonic throat is related to H_m^* by

$$\frac{H_m^*}{H_s^*} = \sigma\left(\overline{M}_m\right), \tag{2.22}$$

where $\overline{M}_m$ is the average Mach number immediately behind the Mach stem.

Through the three-shock theory the flow parameters in the region 1, 2 and 3 (figure 6*d*) are known. The shape and position of the leading part of slipline (before point B), as well as the intensity and the direction of the expansion waves R_s produced over it is solved using the model in § 2.2.2 independently. In addition, the interaction of expansion waves R_c and the reflected wave r can also be solved independently using the model in § 2.2.3. Now the flow conditions in the left and on the top of the wave interaction region are known. The flow parameters in the wave interaction region can thus be solved using the models provided in §§ 2.2.3 and 2.2.4 and following a sequence from left to right and from top to bottom. The expansion fan R_c and the slipline generated waves (R_s and C_s) are represented by a finite number of Mach waves in order to solve the above algorithm.

With the above process, the position and shapes of the slipline s and reflected shock wave r can be obtained. The sonic flow must occur at a section of minimum area. Thus, we examine whether the minimum distance between the slipline and the reflecting surface is exactly equal to H_s^*. If not, we need to update the value of H_m^* and repeat the whole process described above until the exact H_m^* is obtained.

3. Results and discussions

In §§ 3.1–3.2, we will study the flow structure using the model presented in § 2 and compared to CFD, for the case $M_2 > 1$. The case $M_2 < 1$ will be briefly considered in § 3.3. The conclusion of this work is stated in § 3.4.

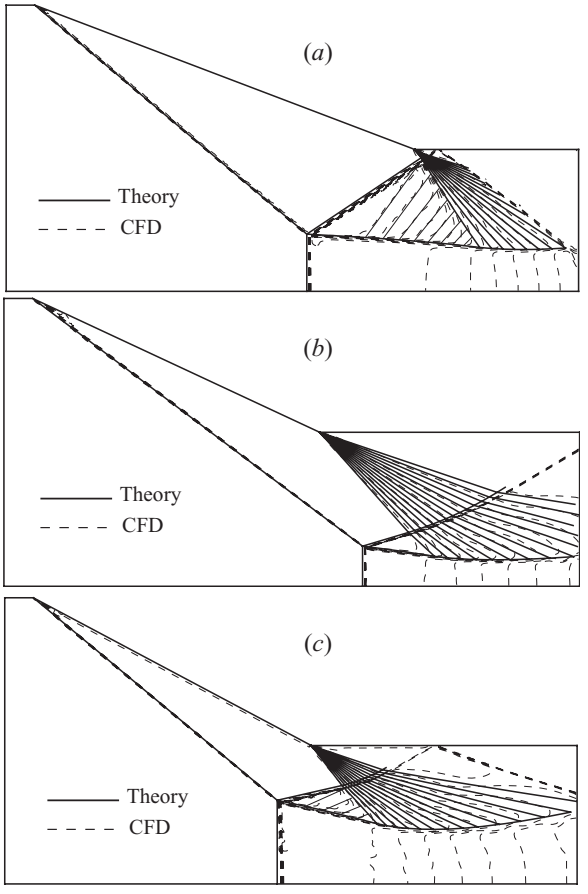

FIGURE 10. Comparison of analytical configuration with the numerical results. (*a*) $M_0 = 2.84, \theta_w = 20.8^\circ, w/H_0 = 1.42$; (*b*) $M_0 = 4.5$, $\theta_w = 25^\circ$, $w/H_0 = 1.1$; and (*c*) $M_0 = 4.96, \theta_w = 28^\circ, w/H_0 = 1.1$.

3.1. *Structure of the flow*

3.1.1. *Overall configuration*

Figure 10(*a*) displays the flow under the conditions $M_0 = 2.84, \theta_w = 20.8$ and $w/H_0 = 1.42$. We observe good agreement between theory and CFD results. In this example, the reflected shock wave is very close to the tail of the wedge surface. Figure 10(*b*) displays a comparison for the case the triple point is near to the transmitted Mach waves under the flow conditions $M_0 = 4.5$, $\theta_w = 25$ and $w/H_0 = 1.1$. Under the influence of the expansion fan, the reflected shock wave deviates upwards gradually. As described in § 2, the influence of the sliplines produced by the interaction of the expansion waves with reflected shock wave are ignored in our prediction. We see from figure 10(*b*) that, the impact of this approximation on the reflection structure is very small. Figure 10(*c*) is a middle state of the above two examples which is under the flow conditions $M_0 = 4.96, \theta_w = 28$ and $w/H_0 = 1.1$. Though the transmitted waves predicted by the theory do not exactly match with the ones obtained by CFD, for which the slipline is oscillatory due to Kelvin–Helmholtz instability, the shape of slipline and reflected shock wave are well predicted by the theory.

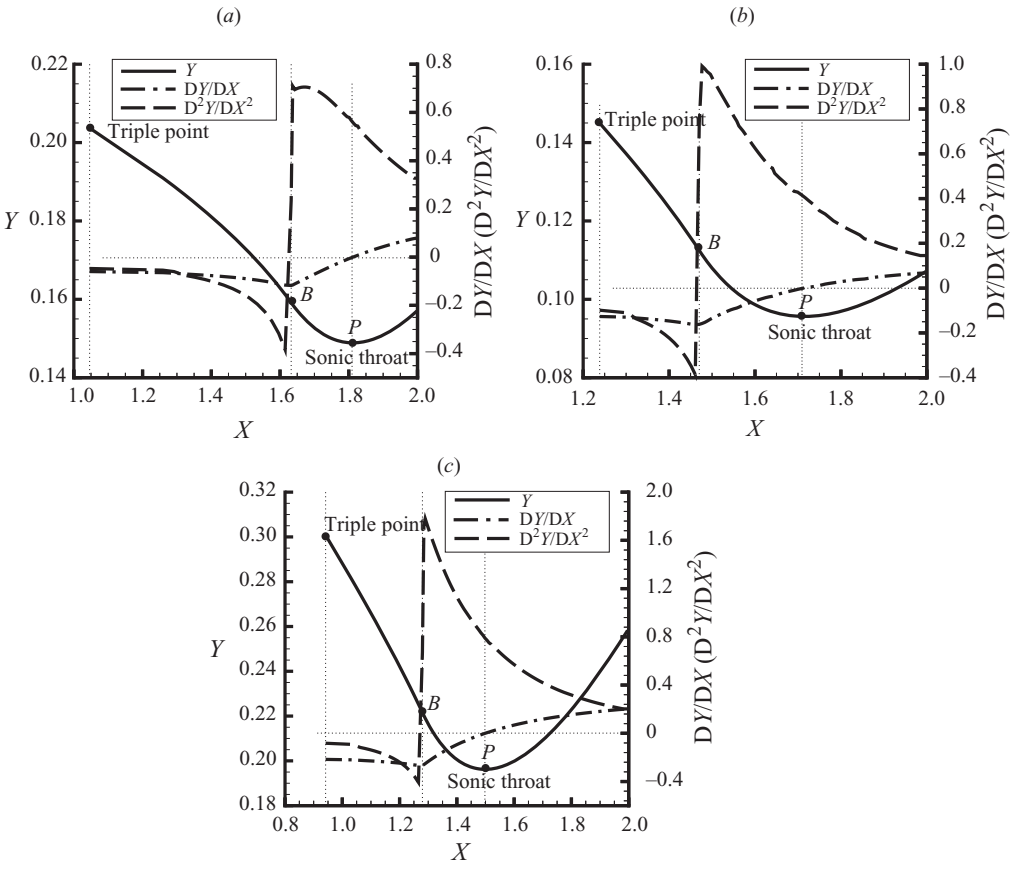

FIGURE 11. Shape and deviation of the analytical slipline. (*a*) $M_0 = 2.84, \theta_w = 20.8^{\circ}$, $w/H_0 = 1.42$; (*b*) $M_0 = 4.5, \theta_w = 25^{\circ}$, $w/H_0 = 1.1$; and (*c*) $M_0 = 4.96, \theta_w = 28^{\circ}$, $w/H_0 = 1.1$.

3.1.2. *Shape of the slipline and the reflected shock wave*

Figure 11 gives the shape and deviation of the analytical slipline for three cases. Across the Mach waves reflected from the slipline, the flow direction deflects downwards. While across the transmitted Mach waves, the flow direction deflects upwards. Therefore, the slipline is first convex and then concave with an inflexion point B where the leading transmitted Mach wave intersects the slipline and the second-order derivative mutates abruptly from negative to positive. Continuously deflecting upwards, the slipline becomes horizontal at point P where the first-order derivative is exactly zero.

Figure 12 displays the pressure gradient along the slipline for $M_0 = 4.5, \theta_w = 25, w/H_0 = 1.1$. In average, the theory follows the CFD results, but the CFD results display oscillation which comes from the oscillatory nature of the slipline, due to Kelvin–Helmholtz instability. This supersonic disturbance transmits downstream in a fixed direction (upper right), spoiling the transmitted waves from the reflected shock wave (see figure 3). This role of the oscillating slipline, observed in CFD, is not covered out by the theory, which may be the main cause for difference (though slight) between theory and CFD.

Figure 13 gives the shape and deviation of the analytical reflected shock wave for two cases. Before interacting with the expansion fan, the reflected shock wave

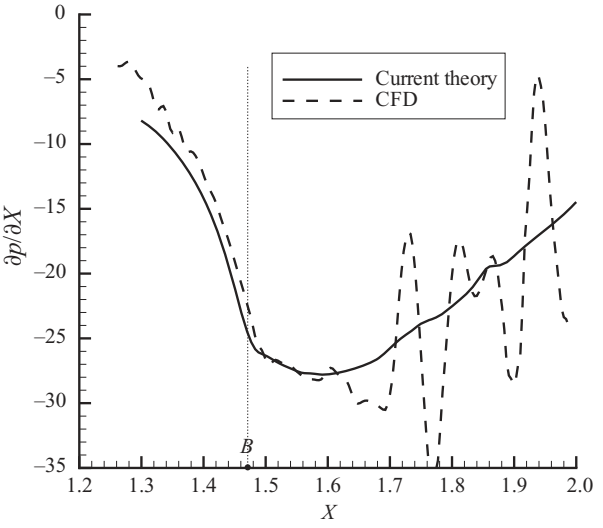

FIGURE 12. Pressure gradient in the throat, $M_0 = 4.5, \theta_w = 25^\circ, w/H_0 = 1.1$.

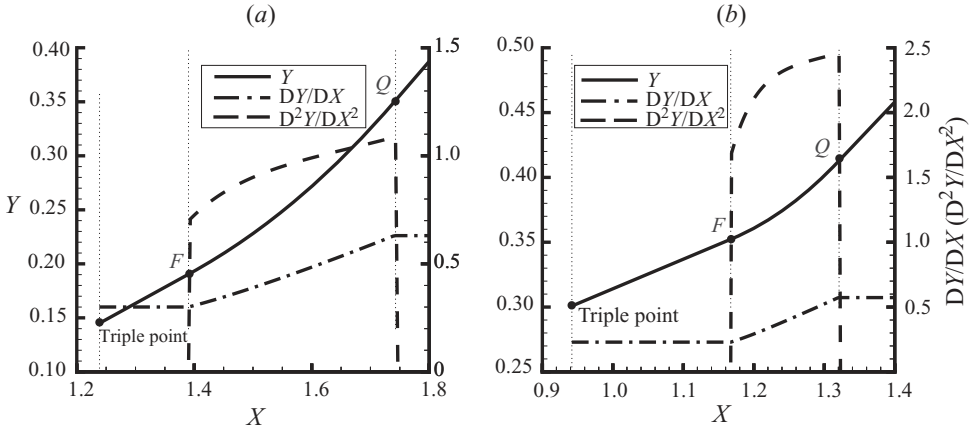

FIGURE 13. Shape and deviation of the analytical reflected shock wave.
(*a*) $M_0 = 4.5, \theta_w = 25^\circ, w/H_0 = 1.1$; (*b*) $M_0 = 4.96, \theta_w = 28^\circ, w/H_0 = 1.1$.

maintains a straight line. The reflected shock wave becomes to deviate upwards from point F where the leading Mach wave intersects it. The first-order derivative begins to increase and the second-order derivative mutates abruptly from zero to a positive value. Due to the interaction with the expansion wave, the reflected shock wave becomes weaker gradually and deviates upwards more seriously. Thus, the second-order derivative increases gradually. The reflected shock wave become straight form point Q where the last Mach wave intersects it. At the very moment, the first-order derivative becomes a constant and the second-order derivative dips to zero.

3.2. *Height of the Mach stem*

As a by-product, the present model also yields a Mach stem height. A comparison of the normalized Mach stem height H_m/H_0 between the present analytical results and those of Li & Ben-dor (1997) and Mouton & Hornung (2007) is shown in table 1. In addition, the CFD results are added to this table. When compared with the CFD

	H_m/H_0						
	CFD					Theory	
Case	M_0	θ_w	w/H_0		Current	Li & Ben-dor (1997)	Mouton & Hornung (2007)
1	2.84	20.8	1.42	0.191	0.202	0.118	0.140
2	4.0	23.0	1.28	0.110	0.121	0.076	0.106
3	4.0	25.0	1.19	0.213	0.223	0.167	0.300
4	4.5	23.0	1.10	0.052	0.058	0.036	0.051
5	4.96	28.0	1.10	0.283	0.292	0.269	0.395
6	5.0	26.9	1.10	0.203	0.213	0.191	0.296

TABLE 1. Mach stem height for various conditions.

results, the present predictions seem to be better than those of Li & Ben-Dor (1997) and Mouton & Hornung (2007) for most of the conditions. This comparison should not be interpreted as superiority of one model over the others. The previous models have the advantage of simplicity while leading to useful results. The present study shows that the deviation of the previous models from CFD results come from the ignorance of the waves over the slipline.

Figure 14 displays a comparison of the present results with those of Li & Ben-dor (1997), of Mouton & Hornung (2007) and current CFD results. the wedge angle is maintained at a fixed value in figures 14(*a*) and 14(*b*), and the free-stream Mach number is maintained at a fixed value in figures 14(*c*) and 14(*d*). It appears that the agreement between the current predictions and the current CFD results is better than others except the case when the Mach stem height is very small. The main reason may be attributed to the difficulty in the determination of the location of the sonic-throat near the von Neumann transition point and the numerical code used.

One additional test example is with $M_0 = 3.98$ and $H_t/L = 0.37$, for various values of θ_w. This test case has been considered by several authors. We compare the present prediction not only with those of Li & Ben-Dor (1997) and Mouton & Hornung (2007), but also with the earlier prediction of Azevedo & Liu (1993), experimental data of Hornung & Robinson (1982) and CFD results of Vuillon *et al.* (1995). It is shown in figure 15 that, the predicted Mach stem height is a little higher than the experimental data. Actually, the height of the Mach stem is highly dependent on the geometry of the test wedge models in experiments. Irving Brown & Skews (2004) pointed out that the Mach stem height decreases with the aspect ratio due to the three-dimensional relieving effect, where the increase in lateral flow relieves the pressure over the surfaces of the wedges. In overall, there is a great discrepancy between various CFD and experimental results around $\theta_w = 23$, possibly due to the three-dimensional effect in experiment or due to the lack of grid convergence in the very early CFD computation. Despite of these uncertainty by early CFD or experimental results, our prediction appears to follow better the data for most of the conditions. Though our model slightly overestimates the Mach stem height, the error appears to be uniform for all conditions.

Figure 16 shows the contour lines of the Mach stem height depending on the wedge angle θ_w and the free-stream Mach number M_0 based on the present prediction under the condition $w/H_0 = 1.1$. The Mach stem height is zero at the von Neumann transition point and increase with M_0 and θ_w. It is important to note that the MR

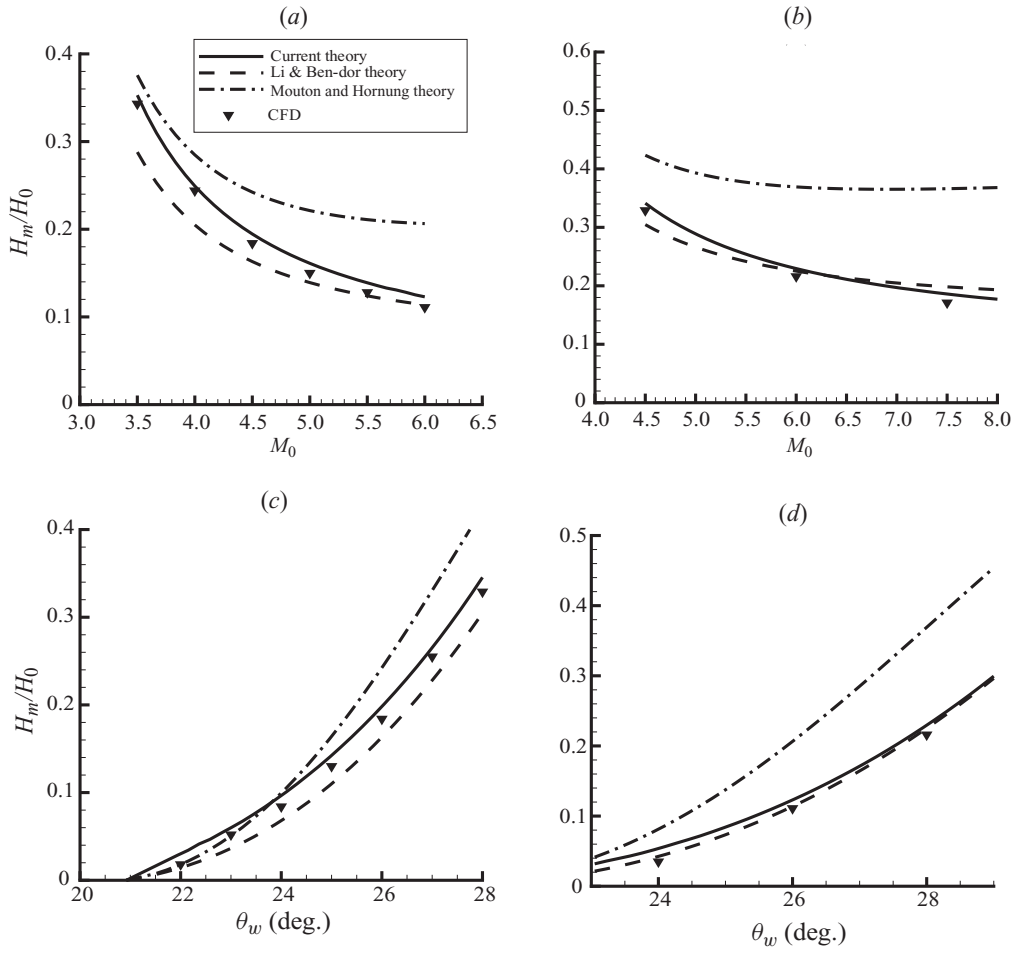

FIGURE 14. Comparisons of the current non-dimensional Mach stem height with those of Li & Ben-dor (1997), of Mouton & Hornung (2007) and current numerical results ($w/H_0 = 1.1$). (a) $\theta_w = 26^o$, (b) $\theta_w = 28^o$, (c) $M_0 = 4.5$ and (d) $M_0 = 6$.

wave configuration is unstable when its reflected shock wave reaches the wedge surface. This is why a maximum wedge angle θ_{max} exists.

3.3. *The flow field for the case* $M_2 < 1$

Figure 17 displays two CFD results of Mach number contours for $M_2 < 1$. For this case, the MR configuration includes not only the expansion (compression) waves produced over the slipline, their interaction with other flow structure, but also a subsonic region behind the first part of the reflected shock wave. This arises a new flow structure, which is the sonic line. The fact that the subsonic region may interact with the slipline, reflected shock wave, as well as the expansion waves, makes it difficult to study the shape of the sonic line.

The shape and position of sonic lines have been studied by Bloor (1964) for hypersonic blunt body problem, by Sauer (1947) for the design of nozzle throat, and for airfoils at sonic inflow conditions (see e.g. Landau & Lifshitz 1987). The flow near a nozzle throat is isentropic and a small perturbation analysis can be used to determine the sonic line. For hypersonic blunt body flow, the flow immediately

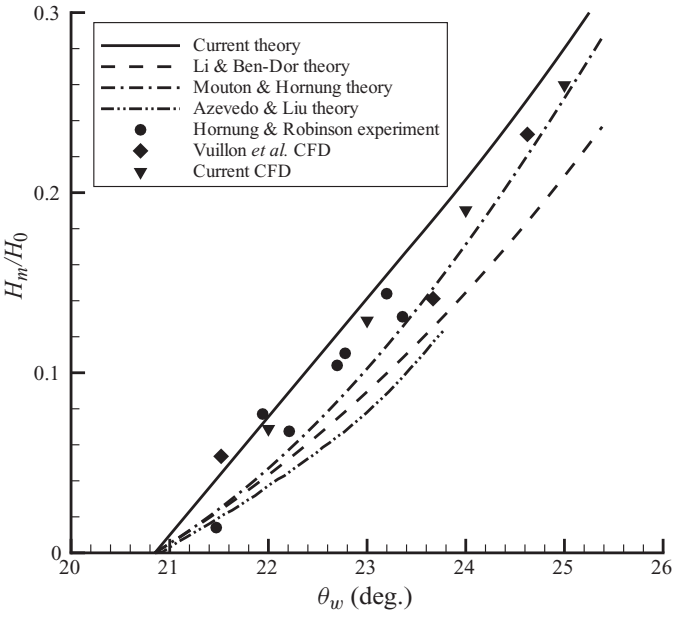

FIGURE 15. Comparisons of the current non-dimensional Mach stem height with those of Li & Ben-dor (1997), of Mouton & Hornung (2007) and of Azevedo & Liu (1993), measurements by Hornung & Robinson (1982) as well as computation by Vuillon *et at*. (1995), $M_0 = 3.98$, $H_t/L = 0.37$.

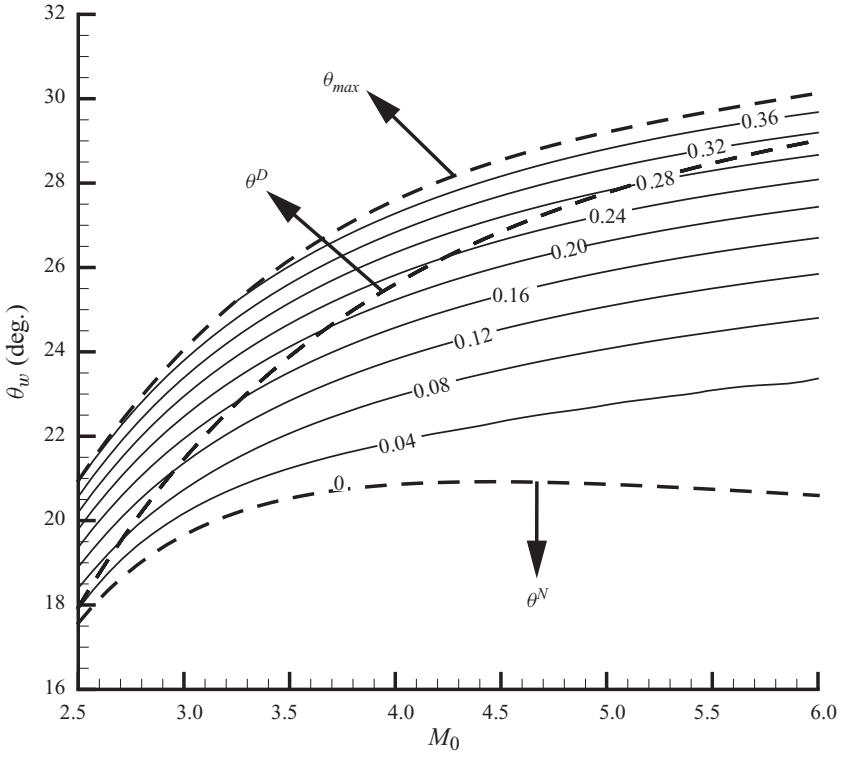

FIGURE 16. The contour lines of Mach stem height, $w/H_0 = 1.1$.

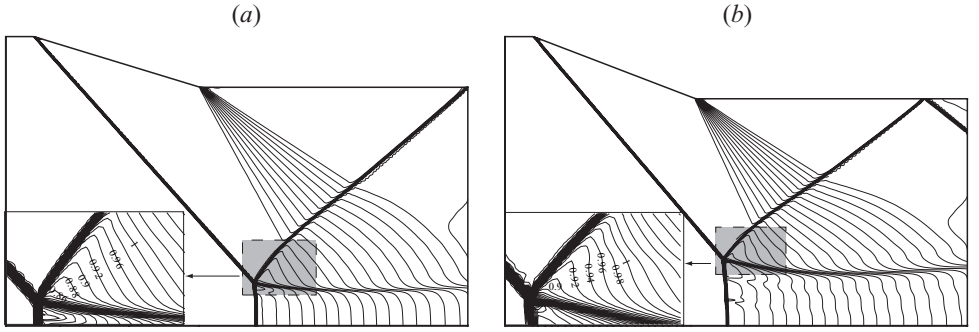

FIGURE 17. Mach number contours for $M_2 < 1$. (*a*) $M_0 = 2.0, \theta_w = 17^\circ, w/H_0 = 0.6$, and (*b*) $M_0 = 2.2, \theta_w = 21^\circ, w/H_0 = 0.6$.

behind the detached shock can be treated by an extended Newtonian theory and only near the body surface this theory should be modified, through expansion in terms of stream function in Bloor (1964). As a result, the sonic line is perpendicular to the wall near the body. For airfoils, the asymptotic behaviour of the sonic line at infinity can be found in Landau & Lifshitz (1987).

For the present Mach reflection problem, the subsonic flow behind the reflected shock wave is non-isentropic so that the transonic small disturbance theory does not hold. The sonic line problem for the MR appears to be more difficult than the above three cases, for which the sonic line is bounded, at least at one end, by the wall. In the present problem the sonic line is embedded in a region which itself has unknown boundaries (slipline and shock waves) to be coupled with the entire flow.

The non-uniformity of the subsonic flow is supposed to be caused by the converging of the flow tube below the slipline, which is assumed to be straight here (its curving is supposed to be of secondary importance). Hence the pressure along the slipline can be roughly modelled by the quasi-one-dimensional theory

$$\frac{p_s}{p_{T_3}} = \chi\left(M_{T_3}, M_s\right), \quad \frac{H_s(\xi)}{H_s^*} = \sigma(M_s), \tag{3.1}$$

where M_s is the mean Mach number below the slipline and T_3 is the point behind the Mach stem and immediate to the triple point. Knowing H_s^* the above relations lead to the pressure and Mach number distributions $p_s = p_s(\xi)$ and $M_s = M_s(\xi)$ at ξ along the slipline.

Immediately above the slipline the flow is assumed to be isentropic (since the slipline is also a streamline) so that we have

$$\frac{p_s}{p_{T_2}} = \chi\left(M_{T_2}, M_{s,a}\right), \quad \frac{p_s}{p_{T_2}} = \frac{\rho_{s,a}^{\gamma}}{\rho_{T_2}^{\gamma}}, \tag{3.2}$$

where $\rho_{s,a}$ and $M_{s,a}$ are the density and Mach number immediately above the slipline, respectively and T_2 is the point behind the reflected shock wave and immediate to the triple point. From (3.1)–(3.2) we obtain

$$p_{T_2}\chi\left(M_{T_2}, M_{s,a}\right) = p_{T_3}\chi\left(M_{T_3}, M_s(\xi)\right), \tag{3.3}$$

from which we can solve for ξ_s (s_1 in figure 6*c*), the sonic point on the slipline, by letting $M_{s,a} = 1$, or $p_{T_2}\chi(M_{T_2}, 1) = p_{T_3}\chi(M_{T_3}, M_s(\xi_s))$.

The quasi-one-dimensional theory is suitable for the region not close to the Mach stem. Unfortunately, the subsonic region behind the reflected shock wave is usually

relatively small, and the sonic point on the slipline is near to the triple point. For this case, the pressure obtained from the quasi-one-dimensional theory is not very accurate. Here, we also use the flow field obtained by Tan *et al.* (2006), based on the small-disturbance equation and is effective in the region not far away from the Mach stem, to determine the pressure along the slipline. The velocity in the subsonic pocket behind the Mach stem is (Tan *et al.* 2006)

$$\left.\begin{aligned} V_x &= V_0 + \frac{\left[(\gamma-1)M_0^2+2\right]\left[2\gamma M_0^2-(\gamma-1)\right]}{H_m(\gamma+1)^2\left(M_0^2-1\right)} a_0\theta_{T_3}(x-x_T), \\ V_y &= -\frac{(\gamma-1)M_0^2+2}{\gamma+1}\frac{\theta_{T_3}}{H_m}a_0 y. \end{aligned}\right\} \tag{3.4}$$

Here, θ_{T_3} is the deflection angle across the Mach stem at the triple point.

Along the slipline, the flow is isentropic and the total enthalpy is a constant, thus we have

$$\begin{aligned} \rho_s &= \rho_{T_3}(p_s/p_{T_3})^{1/\gamma}, \frac{2\gamma}{\gamma+1}\frac{p_s}{\rho_{T_3}(p_s/p_{T_3})^{1/\gamma}} + \frac{\gamma-1}{\gamma+1}(V_x+V_y)^2 \\ &= \frac{2\gamma}{\gamma+1}\frac{p_{T_3}}{\rho_{T_3}} + \frac{\gamma-1}{\gamma+1}M_{T_3}^2 a_{T_3}^2. \end{aligned} \tag{3.5}$$

Considering $y = y_T - (x-x_T)\theta_{T_3}$ and inserting (3.4) in (3.5), we obtain the sonic point on the slipline.

Figure 18 displays the flow under some flow conditions with subsonic flow behind the reflected shock wave. We observe that the sonic point on the slipline predicted by (3.5) is very close to the CFD results. The sonic point on the reflected shock wave appears to be at (at least near) the point the expansion fan (R_c) first intersects the reflected shock wave. Behind the subsonic flow region there are still compression waves generated over the slipline. The reflected shock wave is slightly curved in order to adapt to the pressure decrease along the slipline. This curvature generates entropy waves which transmit the sonic line and then intersect the transmitted Mach waves (R_t). But these entropy waves seem to be weak enough.

Bloor (1965) obtained for the blunt body case that the sonic line is perpendicular to the body (two-dimensional case). If the sonic line is well ahead the transmitted Mach wave (R_t), it should be perpendicular to the slipline from the simple consideration of Mach waves immediately behind the sonic line (since the Mach angle should be $\pi/2$ near sonic point).

However, from the CFD results (figure 18), the sonic line is not perpendicular to the slipline. Rather, it seems to coincide with the leading transmitted wave (R_t). Heuristically, we may explain this should be so. The reflected shock would be weak enough (nature prefers to the weakest solution) so that the subsonic flow region would be as large as possible. If the subsonic pocket should extend to the transmitted expansion waves, then due to the fact the Mach number in the subsonic flow is close to 1, a sudden expansion due to the transmitted Mach waves makes transition to supersonic immediately.

One would be also interested in having a global algorithm to obtain the Mach stem height, similar to the case of $M_2 > 1$. For a fast evaluation of Mach stem height one may follow the integral approach proposed by Chow & Chang (1974) for nozzle free jet flows and for $M_2 < 1$.

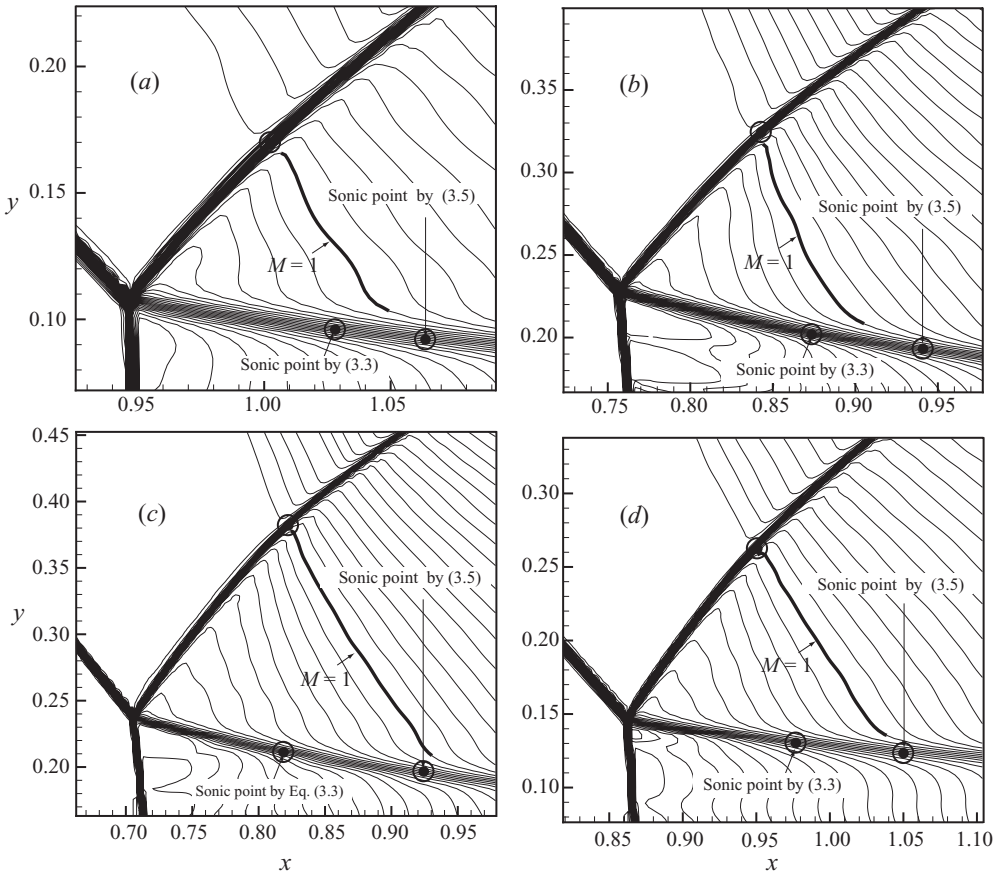

FIGURE 18. Mach contours for $M_2 < 1$ ($w/H_0 = 0.6$). (*a*) $M_0 = 2.2, \theta_w = 19^\circ$, (*b*) $M_0 = 2.2, \theta_w = 21^\circ$, (*c*) $M_0 = 2.0, \theta_w = 19^\circ$and (*d*) $M_0 = 2.0, \theta_w = 17^\circ$.

3.4. *Conclusion*

The inclusion of a series of expansion and compression waves over the slipline, due to the pressure variation below the slipline, is the main contribution of this work. These waves make the flow non-uniform behind the reflected shock wave and determine, jointly with the transmitted expansion waves, the shape of the slipline.

This study not only reveals the non-uniform nature of the flow behind the reflected shock wave, but also shows that the global flow structure, including the Mach stem height, is affected significantly by the slipline generated waves. The former can be used to more reasonably guide CFD study and interpret CFD results. The latter can be used to explain or remedy the departure of previous models from CFD results.

The consideration of the case $M_2 < 1$ reveals interesting features of the sonic line. It appears that the subsonic flow region immediately terminate when encountering the transmitted expansion waves. This is understandable since the Mach number in the subsonic flow pocket is close to 1, so that a sudden expansion (due to transmitted expansion waves) makes it transit immediately to supersonic flow. This means that the sonic line can be simply regarded as in the close vicinity of the first transmitted expansion wave.

The usefulness of this work is the revealing of new flow features and their impact on the global flow structure, though the algorithm is more complicated than the previous models.

The authors are grateful to the referees for their valuable remarks. This work was supported by the Chinese NSF (Contract No. 90716009).

REFERENCES

Azevedo, D. J. 1989 Analytical prediction of shock patterns in a high-speed wedge bounded duct. PhD thesis, Department of Mechanical and Aeronautical Engineering, State University, Buffalo, NY.

Azevedo, D. J. & Liu, C. S. 1993 Engineering approach to the prediction of shock patterns in bounded high-speed flows. *AIAA J.* **31**, 83–90.

Ben-Dor, G. 2007 *Shock Wave Reflection Phenomena*. Springer.

Ben-Dor, G., Elperin, T. & Vasiliev, E. I. 2003 Flow Mach number induced hysteresis phenomena in the interaction of conical shock waves – a numerical investigation. *J. Fluid Mech.* **496**, 335–354.

Bloor, M. I. G. 1965 Determination of the sonic line in hypersonic flow past a blunt body. *J. Fluid Mech.* **21**, 495–501.

Chow, W. L. & Chang, I. S. 1974 Mach reflection associated with over-expanded nozzle free jet flows. *AIAA J.* **13**, 762–766.

Chpoun, A., Passerel, D., Lengrand, J. C., Li, H. & Ben-Dor, G. 1994 Mise en evidence experimentale et numerique d'un phenomane d'hysteresis lors de la transition reflexion de Mach-reflexion reguliere. *Mec. Fluides/Fluid Mech., C. R. Acad. Sci. Paris* **319** (II), 1447–1453.

Chpoun, A., Passerel, D., Li, H. & Ben-Dor, G. 1995 Reconsideration of the oblique shock wave reflection in steady flows. Part 1. Experimental investigation *J. Fluid Mech.* **301**, 19–35.

Dewey, J. M. & Barss, T. 1996 The shape of the Mach stem. In *Proceedings of 12th International Mach Reflection Symposium*, Pilanesberg, South Africa, pp. 263–274.

Dewey, J. M. & McMillin, D. J. 1985*a* Observation and analysis of the Mach reflection of weak uniform plane shock waves. Part 1. Observations. *J. Fluid Mech.* **152**, 49–66.

Dewey, J. M. & McMillin, D. J. 1985*b* Observation and analysis of the Mach reflection of weak uniform plane shock waves. Part 2. Analysis. *J. Fluid Mech.* **152**, 67–81.

Henderson, L. F. & Lozzi, A. 1975 Experiments on transition of Mach reflection. *J. Fluid Mech.* **68**, 139–155.

Henderson, L. F. & Lozzi, A. 1979 Further experiments on transition of Mach reflection. *J. Fluid Mech.* **94**, 541–559.

Hornung, H. G., Oertel, H. & Sandeman, R. J. 1979 Transition to Mach reflection of shock waves in steady and pseudo-steady flows with and without relaxation. *J. Fluid Mech.* **90**, 541–560.

Hornung, H. G. & Robinson, M. L. 1982 Transition from regular to MR of shock waves. Part 2. The steady flow criterion. *J. Fluid Mech.* **123**, 155–164.

Ivanov, M. S., Ben-Dor, G., Elperin, T., Kudryavtsev A. N. & Khotyanovsky, D. V. 2002 The reflection of asymmetric shock waves in steady flows: a numerical investigation. *J. Fluid Mech.* **469**, 71–87.

Irving Brown, Y. A. & Skews, B. W. 2004 Three-dimensional effects on regular reflection in steady supersonic flows. *Shock Waves* **13**, 339–349.

Ivanov, M. S., Gimelshein, S. F. & Beylich, A. E. 1995 Hysteresis effect in stationary reflection of shock waves. *Phys. Fluids.* **7**, 685–687.

Landau, L. D. & Lifshitz E. M. 1987 *Course of Theoretical Physics Vol. 06 Fluid mechanics*. Butterworth-Heinemann.

Li, H. & Ben-Dor, G. 1996 Application of the principle of minimum entropy production to shock wave reflections. I. Steady flows. *J. Appl. Phys.* **80**, 2027–2037.

Li, H. & Ben-Dor, G. 1997 A parametric study of Mach reflection in steady flows. *J. Fluid Mech.* **341**, 101–125.

Li, H., Ben-Dor, G. & Han, Z. Y. 1994 Modification on the Whitham theory for analysing the reflection of weak shock waves over small wedge angles. *Shock Waves J.* **4**, 41–45.

Mach, E. 1878 Uber den verlauf von Funkenwellen in der Ebene und im Raume. *Sitzungsbr. Akad. Wiss. Wien.* **78**, 819–838.

Mouton, C. A. & Hornung, H. G. 2007 Mach stem height and growth rate predictions. *AIAA J.* **45**, 1977–1987.

Olim, M. & Dewey, J. M. 1992 A revised three-shock solution for the Mach reflection of weak shocks ($1.1 < M_i < 1.5$). *Shock Waves J.* **2**, 167–176.

Ren, Y. X. 2003 A robust shock-capturing scheme based on rotated Riemann solvers. *Comput. Fluids* **32**, 1379–1403.

Samtaney, R. & Pullin, D. I. 1996 On initial value and self-similar solutions of the compressible Euler equations. *Phys. Fluids* **8**, 2650–2655.

Shirozu, T. & Nishida, M. 1995 Numerical studies of oblique shock reflection in steady two-dimensional flows. *Mem. Fac. Engng Kyushu Univ.* **55**, 193–204.

Sauer, R. 1947 General characteristics of the flow through nozzles at near critical speeds. *Tech Rep.* TM-1147. NACA.

Tan, L. H., Ren, Y. X. & Wu, Z. N. 2006 Analytical and numerical study of the near flow field and shape of the Mach stem in steady flows. *J. Fluid Mech.* **546**, 341–362.

Teshukov, V. M. 1989 On stability of RR of shock waves. *Prikl. Mekh. Techn. Fiz.* **2**, 26–33.

Von Neumann, J. 1943 Oblique reflection of shock. *Explos. Res. Rep.* 12. Navy Depatment, Bureau of Ordinance, Washington, DC.

Von Neumann, J. 1945 Refraction, intersection and reflection of shock waves. *NAVORD Rep.* 203–245. Navy Department, Bureau of Ordinance, Washington, DC.

Vuillon, J., Zeitoun, D. & Ben-Dor, G. 1995 Reconstruction of oblique shock wave reflection in steady flows. Part 2. Numerical investigation. *J. Fluid Mech.* **301**, 37–50.